International Journal of Innovative Computing, Information and Control
Volume **20**, Number **3**, June **2024**

ICIC International ©2024 ISSN 1349-4198
pp. **911–928**

NOISE SUPPRESSION FOR DAS RECORDS USING THE DOUBLE-SCALE DOUBLE-PATH ATTENTION NETWORK

Tie Zhong[1,2], Hang Yu[2], Wei Wang[3] and Shiqi Dong[1,2,*]

[1]Key Laboratory of Modern Power System Simulation and Control
and Renewable Energy Technology, Ministry of Education
[2]School of Electrical Engineering
Northeast Electric Power University
No. 169, Changchun Road, Jilin 132012, P. R. China
{ zht; 2202200365 }@neepu.edu.cn; *Corresponding author: 20233186@neepu.edu.cn

[3]Institute of Geophysics
Northwest Branch of China Petroleum Exploration and Development Research Institute
No. 561, Yanerwan Road, Lanzhou 730030, P. R. China
wangwei_geophy@petrochina.com.cn

Received August 2023; revised December 2023

Abstract. *Distributed acoustic sensing (DAS) is an innovative acquisition technology that has gradually found application in seismic exploration due to its superior acquisition capabilities. However, the significant amplitude disparity among direct waves, reflected waves, and converted waves in DAS data, coupled with the presence of strong noise pollution, poses major challenges to the subsequent analysis and interpretation of DAS data, ultimately impeding the application and development of the technology. Addressing the need for precise denoising of DAS data, we propose a double-scale double-path attention network (DSDPAN), which extracts effective features through the collaborative representation of information across different scales to enhance its feature expression ability. Under low-scale conditions, DSDPAN employs a method that constructs multiple denoising paths and fuses them based on their correlation to achieve complementary advantages, thereby enhancing denoising performance. Moreover, the spatial attention mechanism is introduced to redistribute the weight of collected features, prioritizing those that are more conducive to noise reduction. The experimental results confirm that DSDPAN outperforms other methods in processing DAS data. After training on a DAS data set consisting of synthetic pure DAS signals and field DAS noise, DSDPAN not only exhibits superior noise suppression capabilities but also achieves effective signal recovery.*
Keywords: Distributed acoustic sensing (DAS), Background noise suppression, Convolutional neural network (CNN)

1. **Introduction.** Distributed acoustic sensing (DAS) is a current technology that uses fiber optic cables as acoustic signal sensors to detect external vibrations [1,2]. Utilizing the sensitivity of optical fibers to vibrations, DAS is capable of capturing environmental vibrations that interact with these fibers [3]. The detailed process is that vibrations change the local properties of the fiber, leading to a shift in the phase of the backward Rayleigh scattered light, consequently modifying the transmitted signal phase. By demodulating the interferometric signal, DAS enables quantitative measurements of the external environment [4]. In recent years, DAS has shown significant potential in seismic exploration, finding widespread applications in seismic imaging [5], seismic inversion [6], reservoir monitoring [7], vertical seismic profiling [8,9], and other related fields. DAS presents numerous

DOI: 10.24507/ijicic.20.03.911

advantages over conventional geophones, including anti-electromagnetic interference, high sensitivity, wide application range, and low cost [10]. Nevertheless, the practical implementation of DAS still encounters challenges. On the one hand, seismic data collected by DAS exhibits a higher complexity level in terms of noise. Specifically, owing to its structural characteristics, the types of inherent instrument noise in DAS are more diverse than those in conventional geophones, such as time-variant optical noise and fading noise, which are absent in conventional geophones [11]. On the other hand, the signal energy acquired by DAS is relatively weaker in contrast to that acquired by conventional geophones. Consequently, the signal is more susceptible to noise interference, posing identification challenges [12]. In summary, DAS is not only affected by complex noise but also constrained by weak signals, resulting in the signal-to-noise ratio (SNR) of seismic data acquired by DAS that is significantly lower than data obtained by conventional geophones. Therefore, the necessity arises to eliminate noise, enhance SNR and attain high-quality DAS records.

In the field of seismic data processing, many classical algorithms have been proposed to be effective in the suppression of noise in data. Early algorithms are widely adopted due to their simplicity and operational ease. For example, the bandpass filter (BPF) removes noise components by retaining only signals within a certain bandwidth [13,14]. And the Fourier transform allows the conversion of time-domain signals, which are difficult to process, into frequency-domain signals that are easier to analyze [15]. Building upon the Fourier transform, the two-dimensional frequency-space (F-K) deconvolution denoising algorithm has been proposed as an effective approach for removing random noise [16,17]. Recent years have witnessed the emergence of innovative and efficacious methods. For instance, a total variation minimization method using texture adaptive based on the partial differential equation algorithm is employed to measure the relationship between texture denoising and texture retention [18-20]. Under the assumption that seismic data usually exhibit redundant structures, a non-local mean denoising algorithm is proposed to identify regions with similar structures and subsequently performs denoising based on these regions [21]. The wavelet transform (WT) has been implemented in seismic signal processing according to its characteristic of multi-scale analysis [22,23]. Empirical mode decomposition (EMD), a decomposition-based technique, separates data into a finite number of intrinsic mode functions, removing noise-related components to achieve denoising [24,25]. Additionally, singular value decomposition (SVD) can effectively eliminate components in seismic observation data that contain strong random noise and surface waves by exploiting the correlation difference between the seismic effective signal and random noise present in each channel [26,27].

However, most of the traditional denoising methods mentioned above are designed for specific noise characteristics and require manual data selection and parameter configuration to estimate the noise level [28]. And these methods often lack local analysis capability, which compromises the original amplitude characteristics of seismic signals, leading to a reduction in signal fidelity [29,30]. In addition, seismic data is characterized by its large size, and the algorithm requires several iterations, resulting in increased complexity [31]. Therefore, the existing traditional methods are insufficient to meet the demand for seismic data denoising, underscoring the need for further exploration of more effective denoising techniques.

With the rapid development of deep learning technology, convolutional neural network (CNN), as one of the representative algorithms, has become a popular research field [32]. For example, frameworks based on CNN have been extensively employed for noise suppression in seismic data, which can be classified into two types: supervised learning

and unsupervised learning [33,34]. The majority of the approaches use supervised learning, which operates on the principle of using labeled datasets for training to establish a mapping relationship between labels and data features. Subsequently, we can utilize the unknown data features to make predictions on the unknown data labels [35,36]. Examples of classical ones include the denoising convolutional neural network (DnCNN) [37] and the residual encoder-decoder deep neural network (RED-Net) [38]. While supervised learning methods emphasize more on the integrity of the training set, unsupervised learning methods have no requirement on the labels and only conduct training according to the loss function or the characteristics of the data itself [39], such as the generating adversarial network (GAN) [40,41]. CNN-based methods have shown superior performance than traditional methods in seismic data processing, thanks to their ability to extract more abstract and efficient information from data using numerous hyperparameters without human intervention [42]. Nonetheless, these methods still have limitations in their capacity to suppress noise and reconstruct signals during experimental processing.

To eliminate the noise in the DAS system, this article applies the multi-scale method and multi-path strategy to processing DAS data and combines the spatial attention mechanism to propose a double-scale double-path attention network (DSDPAN). Specifically, we establish two different scale paths and perform the main feature extraction under low-scale conditions, aiming to acquire deeper information while reducing the training burden. Meanwhile, we implement inter-scale information exchange to facilitate the constant interaction of feature information according to the correlation of information between different scales, which not only complements the loss of the low-scale path in feature extraction but also realizes multi-scale feature extraction. Additionally, we propose a dual-path architecture that collaboratively integrates residual network (Res-Net) [43] and dense network (Dense-Net) [44] to bolster feature extraction capability by combining their respective advantages. To enable the adaptive feature attention allocation, the spatial attention mechanism is incorporated into the DSDPAN framework. Comparative experiments leveraging synthetic DAS recordings and field DAS recordings are conducted to evaluate the denoising performance of DSDPAN. The experimental results demonstrate the superiority of DSDPAN in seismic denoising, as evidenced by its superior performance in noise attenuation and signal reconstruction compared to other methods.

2. **Method.** The specific architecture of DSDPAN is shown in Figure 1, which consists of three different modules: the dual path (DP) module, the spatial attention (SA) module, and the feature communication (FC) module. Specifically, a downsampling operation is executed to create branches of varying scales after increasing the number of channels. Multiple DP modules are introduced to extract a series of features under low-scale conditions. Moreover, the FC module is added to the feature extraction process to make the extracted depth information communicate with the shallow information, thereby averting the loss of critical information. The features gleaned at the low scale are then fed into the SA module to enhance meaningful information. Compared with conventional CNN frameworks (e.g., DnCNN and RED-Net), DSDPAN aims to use multi-scale architecture

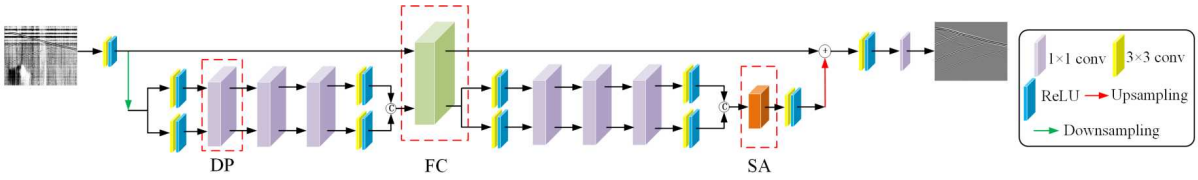

FIGURE 1. DSDPAN architecture

to extract the potential features of the seismic data at different resolutions. The detailed depiction of the network module is presented as follows.

2.1. **Dual path module.** The Res-Net architecture employs skip connections to extract features, establishing a direct link between input and output. The core of Res-Net is the residual block, shown in Figure 2(a). This block passes the features that have been extracted from the previous layer in their entirety to the next layer by performing a point addition operation [45]. Dense-Net is built by densely connecting all layers above to all layers below in a feedforward manner. Specifically, each layer takes the outputs of all previous layers as inputs and further processes them. The foundational structure of the Dense-Net is the dense block, shown in Figure 2(b). The connection between input and output is no longer point-plus but connected in channel dimension [46]. Comparing the principles of Res-Net and Dense-Net, we can analyze their merits and drawbacks. Due to the presence of skip connections, each layer in Res-Net possesses different features, resulting in relatively low feature redundancy. However, this setup also leads to a relatively high rate of feature reuse. The concatenation operation in Dense-Net may result in feature redundancy as later layers could extract features already extracted by earlier layers. Nonetheless, this characteristic empowers Dense-Net with its distinct advantage in mining for new features. To overcome their limitations and achieve the purpose of complementary advantages, we combine them to form the DP module. The fusion strategy shown in Figure 2(c) involves the establishment of a residual path and a dense path, which share convolutions for feature extraction before being returned to their respective paths through two 1×1 convolutions.

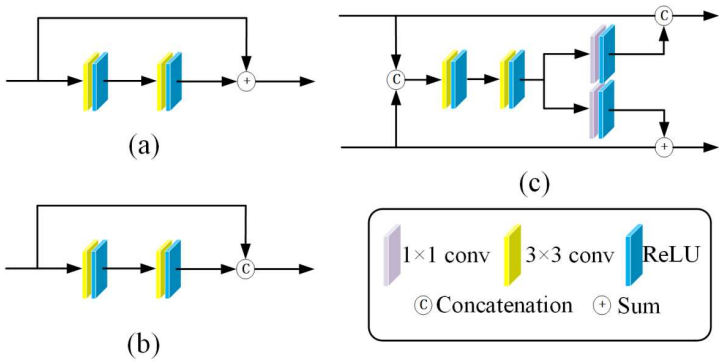

FIGURE 2. DP module architecture: (a) The residual block; (b) the dense block; (c) the architecture

2.2. **Feature communication module.** DSDPAN employs downsampling to create two paths with different scales. Feature extraction in multi-scale scenarios is beneficial for obtaining more detailed information. To transfer information between two scales, the FC module is introduced, which allows the two scales to complement each other and prevents critical features from being ignored during denoising. The structure of the module is shown in Figure 3, where the high-scale and low-scale paths are downsampled and upsampled respectively to match the scales of the other. The acquired results are then integrated with their counterpart path, and the mutual addition process is iterated after the convolution, ultimately achieving information exchange across different scales.

2.3. **Spatial attention module.** Traditional convolutional neural networks treat all features equally, but not all acquired features are favorable for noise reduction. The lack of recognition and learning capability ultimately restricts the expressiveness of deep

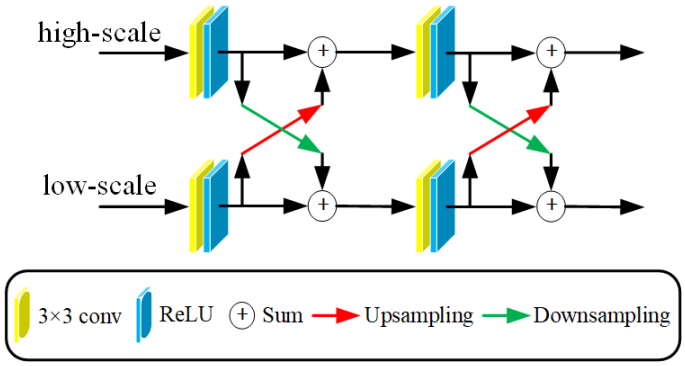

FIGURE 3. FC module architecture

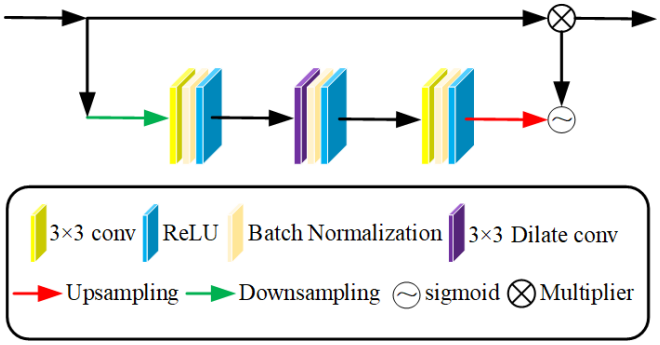

FIGURE 4. SA module architecture

networks. The role of the attention mechanism is to identify what needs attention and then devote additional attention resources to obtain more detailed information while suppressing irrelevant information [47,48]. Based on different principles, it can be divided into channel attention and spatial attention. In this article, we use the spatial attention module to achieve selective attention to the region of interest in the spatial domain. The specific operation, depicted in Figure 4, involves the downsampling of the input along the channel dimension. Moreover, we use an SA module, consisting of two 3×3 convolutional layers and one 3×3 dilated convolutional layer, to generate spatial attention feature maps. The data size is then recovered through upsampling, and the resulting spatial attention feature maps undergo processing with the sigmoid function to ensure the final weight falls within the range of 0 to 1. Finally, the effective information is focused on by multiplication of the input with the final spatial attention feature maps.

2.4. **Denoising principle.** Noise as an interfering factor in the data, can have a detrimental impact on data quality and complicate subsequent processing. Depending on the correlation between noise and pure data, it can be classified into additive and multiplicative noise. Within DAS data, noise predominantly originates from the process of data acquisition and transmission, which belongs to additive noise. Therefore, the mathematical representation of noisy DAS data is as follows:

$$y = x + n \tag{1}$$

where x and n represent theoretically pure DAS data and pure noise data, respectively. We use CNN to effectively separate signal and noise. The denoising process is to build an appropriate network and train it to establish a nonlinear mapping relationship between noisy data and pure data. The entire denoising process can be expressed as

$$\hat{x} = G(y; \theta) \tag{2}$$

where $\hat{x}$ is the estimated signal after denoising, and θ is the hyperparameter, including weight and deviation. The purpose of training involves adjusting the hyperparameter through a large amount of data, so that $\hat{x}$ and x are infinitely close. The loss function is used to guide network training to achieve this purpose. The formula is as follows:

$$\min_\theta loss = \frac{1}{2T}\sum_{i=1}^{T}\|x_i - G(y_i;\theta)\|^2 \tag{3}$$

where x_i represents the label, y_i represents the input, and T is the batch size. After training, the parameter reaches the optimal value θ_{opt}. Therefore, the final result of denoising $\hat{x}_f$ is as follows:

$$\hat{x}_f = G(y;\theta_{opt}) \tag{4}$$

2.5. **Parameter settings.** Taking account of both computational efficiency and modeling accuracy, we have constructed a DSDPAN network composed of six DP modules, one FC module, and one SA module. In the training process, we execute 60 rounds of training with the label of the pure signal. Network optimization is conducted through the Adam optimizer with a batch size of 32, employing learning rates $[10^{-4}, 10^{-5}, 10^{-6}, 10^{-7}]$. We implemented DSDPAN in MATLAB 2017b, and all the training and testing activities were performed on a computer equipped with an Intel(R) Core(TM) i5-9300H CPU @ 2.40GHz and an Nvidia GeForce GTX 1050 GPU.

2.6. **Training set construction.** The efficacy of deep learning networks depends on the availability of big data. A training set with extensive coverage can significantly improve the quality of data processing. The training set used in this study consists of the pure DAS signal set and the DAS noise set. During the training process, signal slices and noise slices are randomly selected from their respective sets and combined, resulting in the construction of noisy DAS data with different levels of noise as input to the network. The process of constructing the pure DAS signal set and DAS noise set is detailed below.

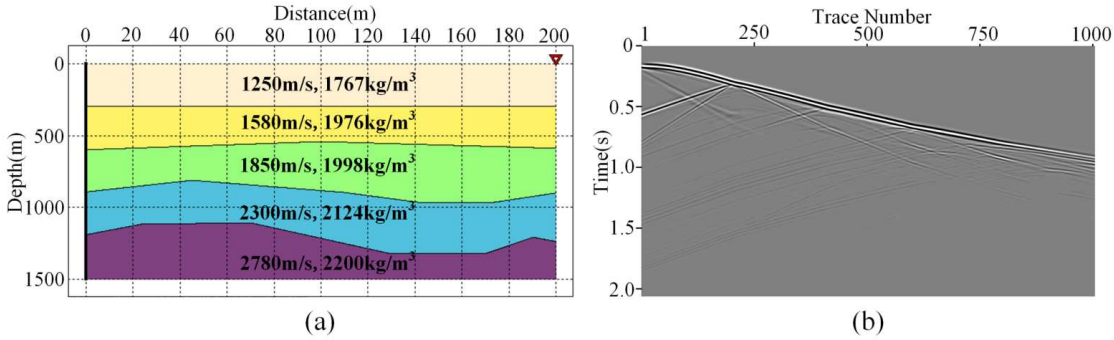

FIGURE 5. Construction of noise-free synthetic record: (a) Forward model; (b) the synthetic record

Due to the unavoidably accompanied noise in the field DAS seismogram, obtaining pure seismograms for the training set construction is unfeasible. For this reason, we generate the pure DAS signal set using seismic forward modeling. The specific process involves first establishing a forward model that accurately reflects the lithology and geological structure of the strata, followed by solving the acoustic wave equation using finite difference methods to simulate the propagation of seismic waves within the strata. Figure 5(a) shows a typical forward modeling scenario, with the receiver represented as a black vertical line and the artificial hypocenter location indicated by a red arrow. The pure DAS data is obtained by receiving the reflected signal using the receiver. Figure 5(b) displays the pure DAS record

TABLE 1. The parameters of forward modeling

Parameters	Specifications
Seismic wavelet	Ricker
Dominant frequency	20-100
Wave velocity	1000-5000 m/s
Well depth	1000-4000 m
Receivers position	Vertical line
Wave equation	Elastic
Trace interval	1 m

generated by this forward model. To improve the generalization of the training set, we set up 100 forward models, meticulously detailed in Table 1. Finally, using the 64×64 sliding window, we extract 18953 signal slices from these pure DAS records, composing the pure DAS signal set.

Acquisition of DAS data in the field is constrained by the accuracy of the instrument and the acquisition technology, which can result in a strong influence of various intrinsic instrument noise and complex environmental noise. Consequently, interference noise often exhibits complex characteristics, which to some extent contributes to the difficulty of suppressing DAS noise. To accurately estimate DAS noise and disentangle noise from the effective signal, the construction of a comprehensive noise set is imperative. We directly obtain the noise from the DAS field data to ensure its authenticity. Similar to the process of establishing the pure DAS signal set, we intercept 38637 noise slices from the noise records using the 64×64 sliding window, thus generating the noise set.

3. **Synthetic Data Denoising Results.**

3.1. **Synthetic test data.** We process the synthetic record to evaluate the denoising performance of DSDPAN. In a similar way to the construction of the training set, the synthetic record comprises both pure DAS data and noise. The pure DAS data is generated through forward modeling. To ensure the reliability of denoising results, the forward model and noise used for testing should not be included in the training set. The specific forward model scenario shown in Figure 6(a) simulates four strata with a depth of 1200 m, featuring progressively increasing wave velocities from top to bottom: 1310 m/s, 1750 m/s, 2300 m/s, and 2830 m/s respectively. An analog source is located 200 m away from the receiver. After excitation, the receiver obtains a noiseless DAS record as shown in Figure 6(b). Based on the noise distribution of actual data, typical DAS noise is incorporated into Figure 6(b) to produce the noisy DAS data as depicted in Figure 6(c). The resulting

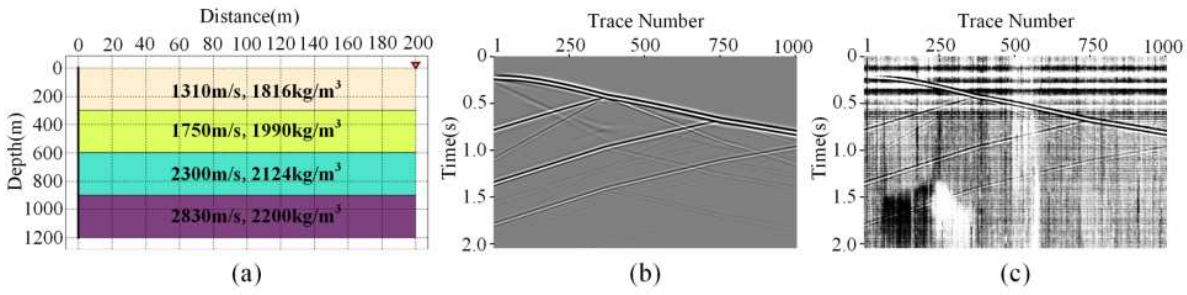

FIGURE 6. The synthetic records used for analysis: (a) Forward model; (b) pure record; (c) noisy record

noisy data bears an SNR of −5 dB. It can be seen that strong background noise contaminates effective signals, causing weak signals to become submerged and difficult to identify.

3.2. **Experimental results.** We employ two traditional methods with different principles to process the synthetic record: BPF and ensemble empirical mode decomposition (EEMD). In addition, we use four CNN methods: DnCNN, Res-Net, Dense-Net, and a novel multi-scale DnCNN (MSDCNN) [49]. The denoising results of DSDPAN are compared with those of the aforementioned methods to verify the rationality of the proposed method. For the accuracy of the experiment, the training of the five CNNs is executed under identical conditions. Specific parameters for each network are meticulously outlined in Table 2.

TABLE 2. Training parameters of DnCNN, Res-Net, Dense-Net, and DSDPAN

Hyper-parameter	DnCNN	Res-Net	Dense-Net	MSDCNN	DSDPAN
Optimizer	ADAM	ADAM	ADAM	ADAM	ADAM
Batch size	32	32	32	32	32
Patch size	64×64	64×64	64×64	64×64	64×64
Epoch	60	60	60	60	60
Learning rate range	$[10^{-4} \sim 10^{-7}]$	$[10^{-4} \sim 10^{-7}]$	$[10^{-4} \sim 10^{-7}]$	$[10^{-4} \sim 10^{-7}]$	$[10^{-4} \sim 10^{-7}]$
Input channels	1	1	1	1	1
Layers	$3 \times 3 \times 20$	$3 \times 3 \times 30$	$3 \times 3 \times 30$	$3 \times 3 \times 32$	$3 \times 3 \times 32$, $1 \times 1 \times 13$

The result of the BPF algorithm, as shown in Figure 7(b), has a limited noise suppression effect on horizontal noise and fading noise, despite some effectiveness on random noise and time-variant optical noise. For example, it is difficult to identify weak signals in box A. Figure 7(c) illustrates the result of the EEMD processing, where the effectiveness of noise suppression is comparable to that of BPF. In terms of signal recovery, not only do weak DAS signals remain unrecoverable, but the continuity of strong signals in box

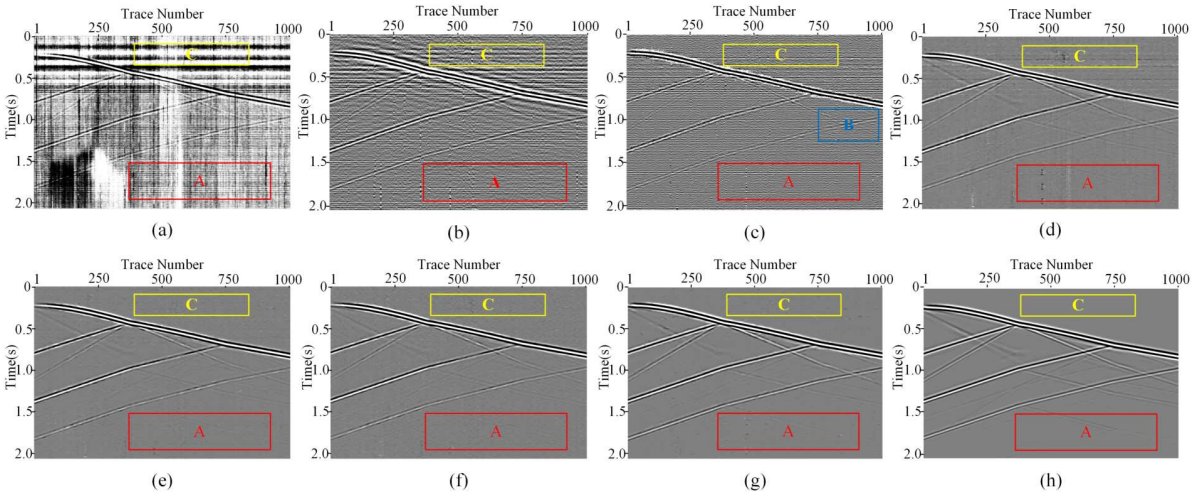

FIGURE 7. Comparisons for denoised results: (a) Synthetic DAS record; (b)-(h) denoised results for BPF, EEMD, DnCNN, Res-Net, Dense-Net, MSDCNN, and DSDPAN

B is compromised. It is evident from these results that traditional denoising techniques have limitations in the processing of synthetic data. DnCNN's denoising result, as shown in Figure 7(d), exhibits a significant improvement over traditional methods in terms of overall denoising effectiveness. However, the reconstitution of signals is still adversely affected by residual horizontal noise and fading noise, thereby compromising its integrity. Res-Net and Dense-Net show similar effects with corresponding processing results presented in Figures 7(e) and 7(f). While most noise has been eradicated, residual noise remains within box C. Furthermore, the continuity of the weak signals is still unsatisfactory, although most of the effective signals can be recovered. The signal recovery effect of MSDCNN shows a slightly stronger performance compared to other competing methods, as depicted in Figure 7(g), where weak signals can be detected to some extent. Figure 7(h) demonstrates that DSDPAN effectively eliminates different types of noise, resulting in a cleaner background and continuous recovery of both strong and weak signals. Experimental results highlight DSDPAN's superiority over alternative processing methods, excelling in both noise suppression and signal recovery.

We analyze pure noise and filtered noise results depicted in Figures 8(a) to 8(h) to evaluate the amplitude-preserving properties of different methods. The filtered noise using the BPF algorithm is displayed in Figure 8(b). The results indicate that the BPF shows a certain degree of amplitude retention capability, with no significant signal residue observed in regions other than some effective signals within box A. Noise results obtained after EEMD, DnCNN, Res-Net, and Dense-Net filtering are presented in Figures 8(c) to 8(f), which exhibit conspicuous signal residue. Although MSDCNN performs better, weak signal leakage still can be observed in Figure 8(g). All these results suggest that their ability to preserve amplitude is inadequate and in need of further improvement. Figure 8(h) demonstrates the noise filtered out by DSDPAN, portraying a relatively clean background without signal aliasing. It is evident that DSDPAN effectively mitigates the attenuation of the signal amplitude. Comparative analysis of experimental results shows that DSDPAN can effectively eliminate noise without compromising desired signal integrity.

To conduct a more comprehensive evaluation of these methods' performance, we introduce the F-K spectrum for comparison in the frequency domain. Figure 9(a) displays the F-K spectrum of the pure recording and pure noise, while Figure 9(b) presents the F-K

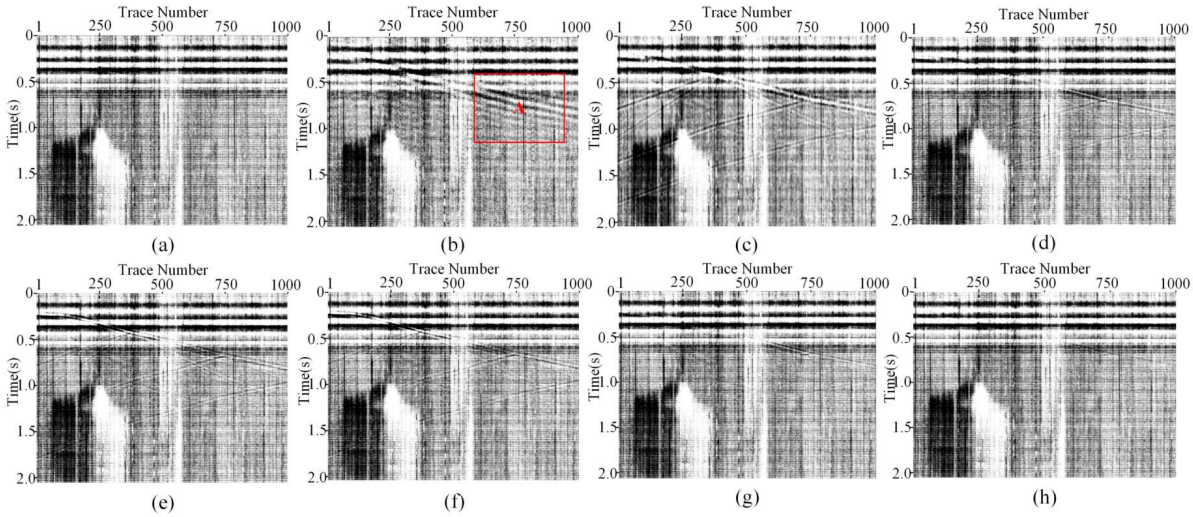

FIGURE 8. Comparisons for filtered noise results: (a) Pure noise; (b)-(h) filtered noise for BPF, EEMD, DnCNN, Res-Net, Dense-Net, MSDCNN, and DSDPAN

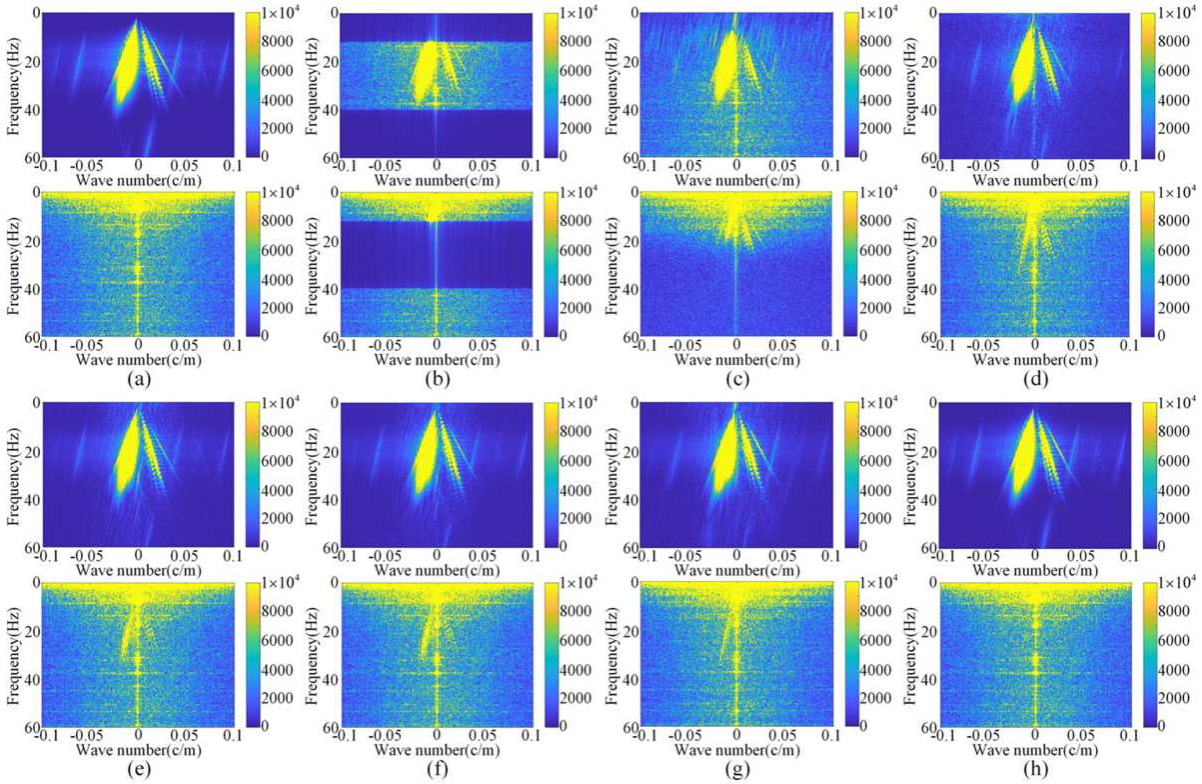

FIGURE 9. F-K spectra for different denoised results: (a) F-K results for pure signals and noise; (b)-(h) F-K results for recovered records (top subfigures) and removed noise (bottom subfigures) obtained by BPF, EEMD, DnCNN, Res-Net, Dense-Net, MSDCNN, and DSDPAN

spectrum of the BPF result. We observe that the BPF retains noise with a frequency similar to that of the target signal, resulting in limited effectiveness for noise removal. The F-K spectrum of the EEMD result in Figure 9(c) shows that EEMD has problems with incomplete noise removal and loss of effective signal. Compared with the two traditional methods, DnCNN (Figure 9(d)), Res-Net (Figure 9(e)), Dense-Net (Figure 9(f)) and MSDCNN (Figure 9(g)) exhibit enhanced noise removal and signal recovery capabilities. Among the four methods, Res-Net and Dense-Net demonstrate excellent performance, providing a cleaner background and managing to recover weaker signals. However, the denoising effectiveness of Res-Net, Dense-Net and MSDCNN remains suboptimal due to their limited noise suppression capability and inability to prevent signal leakage. Figure 9(h) illustrates that DSDPAN has superior noise suppression and amplitude preservation capabilities compared to the methods mentioned above, with denoising results and filtered noise closely resembling pure recording and pure noise in the frequency domain. The F-K spectrum experiment is further confirmation that DSDPAN has more advantages in DAS data processing.

In quantitative analysis, SNR and root mean square error (RMSE) serve as metrics to gauge denoising efficacy. A higher SNR and a lower RMSE represent better denoising performance. We employ six different methods to process synthetic records with different SNR levels. The results are presented in Table 3.

Data analysis indicates that BPF and EEMD fall short of achieving the expected SNR improvement. In contrast, DnCNN, Res-Net, and Dense-Net exhibit heightened noise suppression prowess within DAS data, leading to notable SNR improvement. The seismic records processed by MSDCNN have a higher SNR, indicating that the quality of

TABLE 3. Comparisons of SNR and RMSE for different attenuation methods

Original record/dB		0	−2	−4	−6	−8	−10
BPF	SNR/dB	9.56	8.51	7.25	5.79	4.16	2.42
	RMSE	0.2725	0.3072	0.3554	0.4206	0.5070	0.6197
EEMD	SNR/dB	9.71	8.00	6.19	4.33	2.50	0.63
	RMSE	0.2676	0.3258	0.4017	0.4974	0.6144	0.7614
DnCNN	SNR/dB	12.91	12.09	11.09	9.87	8.37	6.57
	RMSE	0.1851	0.2036	0.2284	0.2628	0.3122	0.3843
Res-Net	SNR/dB	15.47	14.76	13.89	12.90	11.85	10.76
	RMSE	0.1379	0.1417	0.1654	0.1854	0.2093	0.2372
Dense-Net	SNR/dB	15.84	15.04	14.14	13.14	12.03	10.83
	RMSE	0.1321	0.1449	0.1608	0.1805	0.2050	0.2353
MSDCNN	SNR/dB	16.37	15.76	15.02	14.05	12.84	11.34
	RMSE	0.1244	0.1334	0.1453	0.1624	0.1868	0.2222
DSDPAN	SNR/dB	18.08	17.68	17.11	16.33	15.45	14.46
	RMSE	0.1022	0.1070	0.1142	0.1249	0.1382	0.1549
	Improved percentage	10%	12%	14%	16%	20%	27%

the obtained result exceeds those achieved through the aforementioned comparing methods. Compared to other methods, DSDPAN achieves the highest SNR and lowest RMSE results. It demonstrates excellent denoising capability even under low SNR conditions with an improvement of over 24 dB for the −10 dB record. Moreover, the percentage improvement of the DSDPAN method is also calculated to make a clear comparison, and the corresponding results are shown at the bottom of Table 3. Here, MSDCNN, having the best performance in competing methods, is selected as the reference. It is shown that DSDPAN has over at least 10% increment than MSDCNN, and the percentage even raised to 27% for the low-SNR records. In summary, DSDPAN provides optimal noise reduction across different SNR levels.

When applying deep learning to denoising, the computational cost of the algorithm cannot be ignored. DnCNN, Res-Net, Dense-Net and DSDPAN are deep learning methods that require parameter tuning through training to achieve optimal performance, resulting in a high training burden. Specifically, DnCNN and Res-Net have 664,704 and 1,106,048 network parameters, respectively. Due to the increase in the number of channels resulting from dense connections, Dense-Net and MSDCNN generate substantial number of network parameters totaling 2,211,968 and 1,363,968, respectively. In contrast, DSDPAN employs a dual-path strategy to generate a large number of network parameters, with a specific count of 2,503,296. However, DSDPAN primarily performs feature extraction under low-scale conditions, thereby reducing the computational burden. We analyzed computational efficiency by processing 20 synthesis records with different SNRs. Table 4 presents the training time, processing time, and the average SNR improvement achieved by each method. As observed from the table, DnCNN, Res-Net, Dense-Net, MSDCNN, and DSDPAN require 4.67, 6.93, 12.37, 17.52, and 6.65 hours of training time respectively, while BPF and EEMD demand no training. Consequently, the computational cost of deep learning methods far exceeds that of traditional methods. However, after undergoing training, deep learning methods can ensure high processing efficiency. In addition, the deep learning approach manifests a more pronounced improvement in SNR, with DSDPAN yielding an improvement of 25.37 dB. In general, deep learning achieves strong SNR improvement at the expense of high computational costs. As a result, such computational costs are justifiable and can be mitigated by advances in the hardware.

TABLE 4. Comparison of computation cost and improved SNR for different methods

Hyper-parameter	BPF	EEMD	DnCNN	Res-Net	Dense-Net	MSDCNN	DSDPAN
Processing time (s)	0.2637	570.7380	1.3906	1.5078	1.7218	1.9384	1.4300
Training time (hour)	0	0	4.67	6.93	12.37	17.52	6.65
Average improved SNR (dB)	12.06	10.09	15.70	19.97	20.24	22.23	25.37

4. **Field DAS Data Denoising Results.**

4.1. **Field DAS data.** We subject a part of field-acquired DAS records for testing. One of the DAS records, which is employed in testing, is shown in Figure 10(a). It is evident that the complexity of noise types and properties in field DAS records exceeds those in synthetic DAS records, with nearly all signals being annihilated in noise, posing a challenge to seismic event identification.

4.2. **Experimental results.** The denoising results of BPF, EEMD, DnCNN, Res-Net, Dense-Net, MSDCNN, and DSDPAN on field DAS records are compared to verify their effectiveness in complex cases. We use the same training set as the synthetic record experiment to ensure the reliability of the experiment. It is difficult to obtain pure DAS data due to the inevitable noise in the field DAS collection process. Therefore, the realization of quantitative measurement is not feasible, and only qualitative analysis can be conducted.

Noise reduction results of the BPF and EEMD methods on field DAS data are presented in Figures 10(b) and 10(c), respectively. These results indicate that both methods fail to effectively remove noise, evident from the noticeable horizontal noise residue within box A. Furthermore, the overall signal continuity cannot be guaranteed after BPF or EEMD processing. Figures 10(d) to 10(g) display the processing results of four deep learning techniques, which exhibit a cleaner background and a more complete signal compared to those obtained by traditional methods. Among them, DnCNN exhibits weaker denoising performance than that of Res-Net, Dense-Net, and MSDCNN. The result of DnCNN not only contains a significant amount of noise but also fails to recover effective signals in areas affected by strong energy noise. In contrast, Res-Net and Dense-Net can remove most of the noise, but their signal recovery capability remains insufficient. For example, seismic events in the area affected by time-variant optical noise circled by box B are not completely and continuously recovered. In addition, MSDCNN exhibits superior performance in attenuating background noise and improving signal recovery. However, it suffers from a similar issue as Res-Net and Dense-Net in terms of the limited effectiveness of event recovery in regions disrupted by intense noise. The denoising result of DSDPAN is shown in Figure 10(h), which exhibits the best overall noise reduction effect compared to the aforementioned methods, especially for horizontal noise (boxed A), time-variant optical noise (boxed B), and coherent noise (boxed C). Moreover, the overall signal reconstruction is more distinct and continuous.

To allow a more intuitive comparison of the area affected by time-variant optical noise in box B, we have enlarged and presented in Figures 11(a) to 11(h). It can be seen that the clarity and completeness of the effective signals recovered by DSDPAN are significantly superior to those obtained by other methods. The results of the field DAS record processing indicate that DSDPAN has better denoising performance, which is consistent

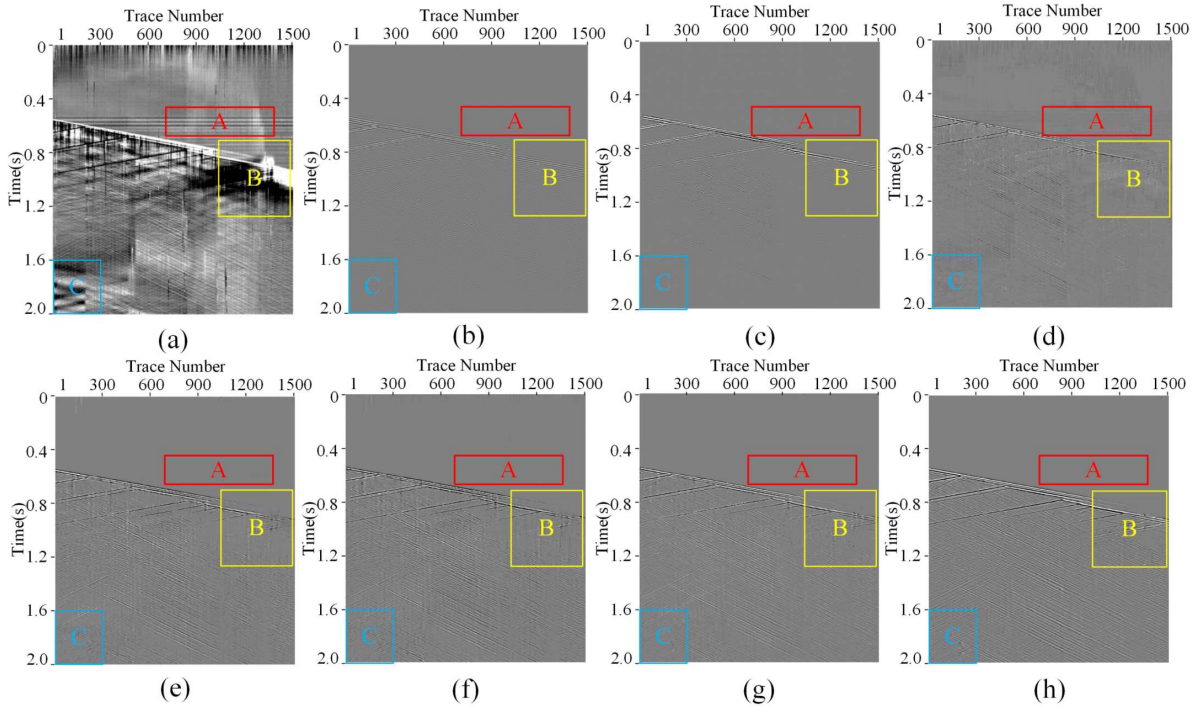

FIGURE 10. Denoised result comparisons for different methods for Scenario 1: (a) Field DAS record; (b)-(h) denoised results for BPF, EEMD, DnCNN, Res-Net, Dense-Net, MSDCNN, and DSDPAN

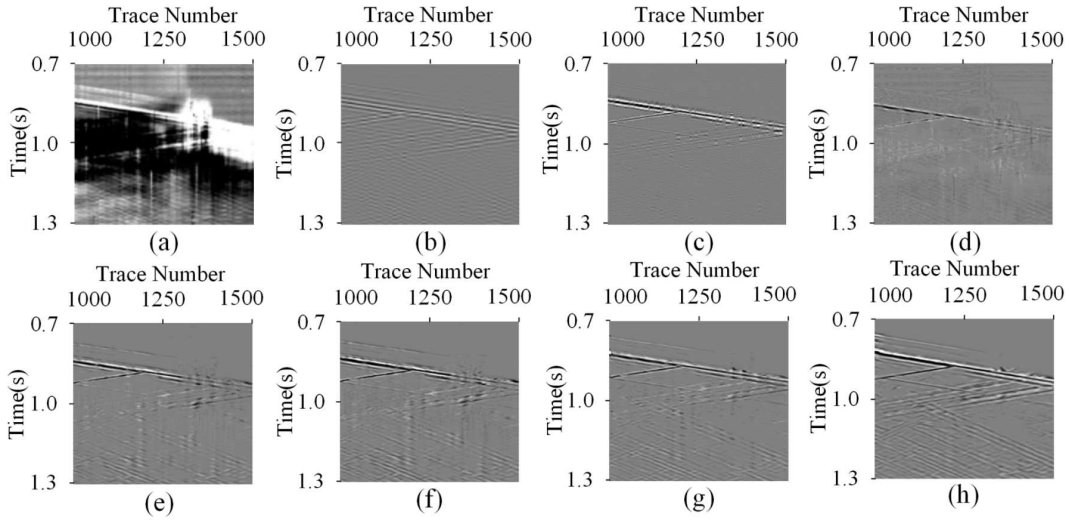

FIGURE 11. Comparisons for enlarged denoised results for Scenario 1: (a) Field DAS record; (b)-(h) denoised results for BPF, EEMD, DnCNN, Res-Net, Dense-Net, MSDCNN, and DSDPAN

with the conclusion of the synthetic DAS record experiment and confirms the rationality and effectiveness of this method.

To assess the generalization of DSDPAN, we used a field DAS record depicted in Figure 12(a) that differs from the previous scenario used for testing. The processing results of seven methods are shown in Figures 12(b) to 12(h). As can be seen from the figures, DSDPAN performs the best performance in suppressing DAS noise, especially in overall fading noise and random noise suppression. Res-Net and Dense-Net have the same effect

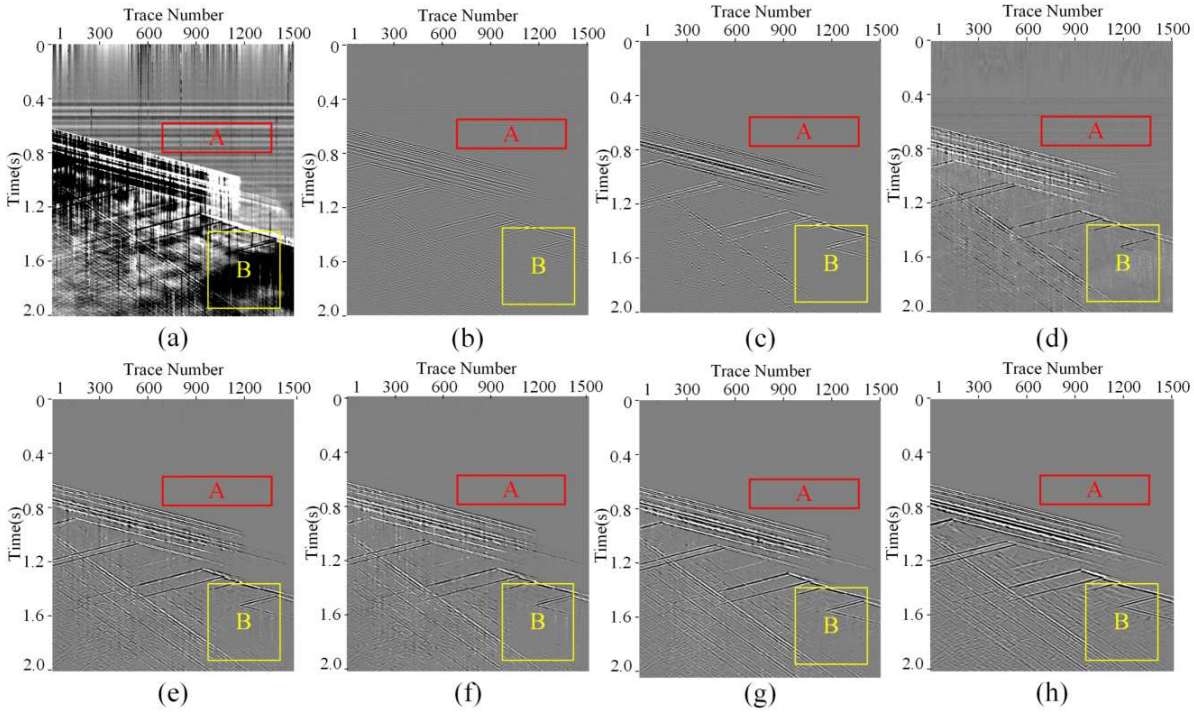

FIGURE 12. Denoised result comparisons for different methods for Scenario 2: (a) Field DAS record; (b)-(h) denoised results for BPF, EEMD, DnCNN, Res-Net, Dense-Net, MSDCNN, and DSDPAN

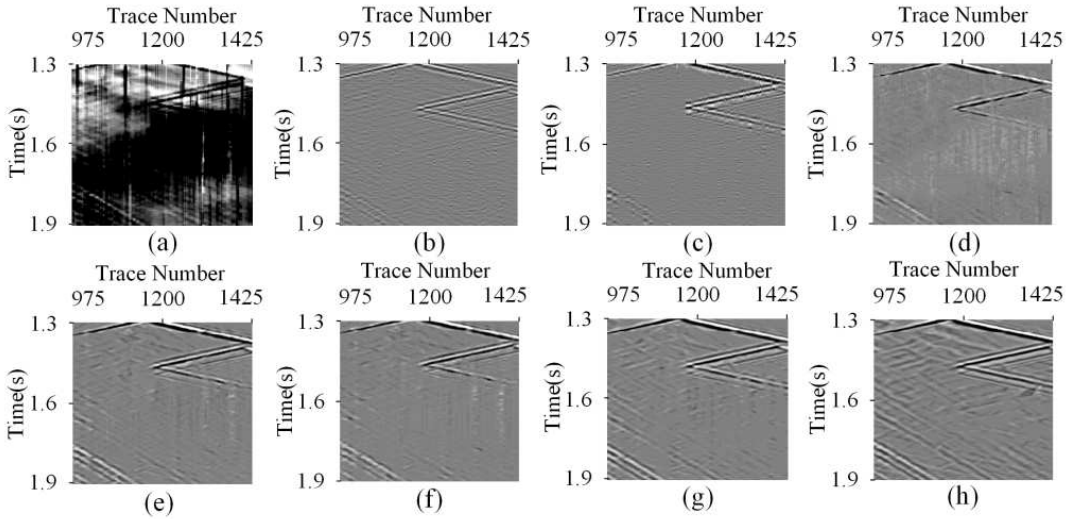

FIGURE 13. Comparisons for enlarged denoised results for Scenario 2: (a) Field DAS record; (b)-(h) denoised results for BPF, EEMD, DnCNN, Res-Net, Dense-Net, MSDCNN, and DSDPAN

on noise attenuation, while BPF, EEMD, and DnCNN fail to achieve satisfactory noise suppression with noticeable residual noise. Meanwhile, although MSDCNN exhibits a slight superiority over other competing methods, the denoising results of field data are still inferior to DSDPAN in the recovery of weak signals.

By zooming in on the area circled by box B, as depicted in Figures 13(a) to 13(h), we can more intuitively observe the signal recovery of these methods. In the results of

BPF, EEMD, and DnCNN, almost no effective signal can be recovered due to the influence of time-variant optical noise. Res-Net, Dense-Net and MSDCNN have certain signal recovery effects, but the signal integrity is still insufficient. DSDPAN is capable of effectively extracting signals from strong noise while ensuring signal continuity. In conclusion, DSDPAN exhibits superior noise suppression capabilities compared to other methods for different field DAS records.

5. **Conclusion.** We propose a novel denoising network, DSDPAN, as a solution to the complex problem of noise pollution in the DAS records. To achieve comprehensive feature acquisition, DSDPAN employs the concept of multi-scale communication, ensuring information transfer across scales while extracting potential features from data of different resolutions. In addition, DSDPAN adopts a multi-path approach, leveraging diverse methodologies to construct multiple paths and combine them to achieve methodological complementarity, thereby enhancing overall performance. The incorporation of the spatial attention mechanism directs more focus toward features that have a positive impact on noise suppression, simplifying complex features. Based on the processing results of synthetic DAS records and field DAS records, it can be observed that DSDPAN effectively suppresses various types of noise in DAS data, not only removing fading noise and random noise but also showing excellent attenuation capability for coherent noise and time-variant optical noise. Furthermore, DSDPAN exhibits superior signal recovery with minimal amplitude loss during the denoising process, resulting in a higher improvement of SNR compared to other methods. In summary, the experimental results have demonstrated the effectiveness of DSDPAN; however, its denoising capability is still sensitive to the quality of the training dataset, as the network is trained in a supervised manner. Meanwhile, the limited performance, caused by extremely strong DAS background noise, and nonnegligible training costs also needs to pay more attention and design efficient network architecture to cope with them. Even so, DSDPAN is a meaningful attempt to utilize a CNN-based method to achieve effective attenuation of intense DAS background noise.

REFERENCES

[1] M. Li, H. Wang and G. Tao, Current and future applications of distributed acoustic sensing as a new reservoir geophysics tool, *The Open Petroleum Engineering Journal*, vol.8, no.18, pp.272-281, 2015.

[2] G. Bellefleur, E. Schetselaar, D. Wade, D. White, R. Enkin and D. R. Schmitt, Vertical seismic profiling using distributed acoustic sensing with scatter-enhanced fiber-optic cable at the Cu-Au New Afton porphyry deposit, British Columbia, Canada, *Geophysical Prospecting*, vol.68, no.1, pp.313-333, 2020.

[3] A. Hartog, B. Frignet, D. Mackie and M. Clark, Vertical seismic optical profiling on wireline logging cable, *Geophysical Prospecting*, vol.62, no.4, pp.693-701, 2014.

[4] J. C. Hornman, Field trial of seismic recording using distributed acoustic sensing with broadside sensitive fibreoptic cables, *Geophysical Prospecting*, vol.65, no.1, pp.35-46, 2017.

[5] K. Harris, D. White and C. Samson, Imaging the Aquistore reservoir after 36 kilotonnes of CO_2 injection using distributed acoustic sensing, *Geophysics*, vol.82, no.6, pp.M81-M96, 2017.

[6] A. Egoro, Elastic full-waveform inversion of vertical seismic profile data acquired with distributed acoustic sensors, *Geophysics*, vol.83, no.3, pp.R273-R281, 2018.

[7] G. Byerley, D. Monk, P. Aaron and M. Yates, Time-lapse seismic monitoring of individual hydraulic frac stages using a downhole DAS array, *The Leading Edge*, vol.37, no.11, pp.802-810, 2018.

[8] K. N. Madsen, M. Thompson, T. Parker and D. Finfer, A VSP field trial using distributed acoustic sensing in a producing well in the North Sea, *First Break*, vol.31, no.11, pp.51-56, 2013.

[9] T. Parker, S. Shatalin and M. Farhadiroushan, Distributed acoustic sensing – A new tool for seismic applications, *First Break*, vol.32, no.2, pp.61-69, 2014.

[10] T. Zhong, H. Chen, S. Dong and J. Li, DAS-VSP noise elimination based on the dilated pyramid attention network, *International Journal of Innovative Computing, Information and Control*, vol.19, no.5, pp.1361-1375, 2023.
[11] S. Wang, Y. Li and Y. Zhao, Attribute-guided target data separation network for DAS VSP data, *IEEE Transactions on Geoscience and Remote Sensing*, vol.60, no.1, pp.1-16, 2022.
[12] G. Binder, A. Titov and Y. Liu, Modeling the seismic response of individual hydraulic fracturing stages observed in a time-lapse distributed acoustic sensing vertical seismic profiling survey, *Geophysics*, vol.85, no.4, pp.T225-T235, 2020.
[13] R. A. Stein and N. R. Bartley, Continuously time-variable recursive digital band-pass filters for seismic signal processing, *Geophysics*, vol.48, no.6, pp.702-712, 1983.
[14] X. Dong, H. Jiang, S. Zheng, Y. Li and B. Yang, Signal-to-noise ratio enhancement for 3C downhole microseismic data based on the 3D shearlet transform and improved back-propagation neural networks, *Geophysics*, vol.84, no.4, pp.V245-V254, 2019.
[15] L. Canales, Random noise reduction, *Proc. of SEG Technical Program Expanded Abstract*, vol.1984, no.1, pp.525-527, 1984.
[16] W. Sun, S. Zhu, W. Li, W. Chen and N. Zhu, Noise suppression of distributed acoustic sensing based on f-x deconvolution and wavelet transform, *IEEE Photonics Journal*, vol.12, no.1, pp.1-8, 2020.
[17] G. Liu, S. Fomel, L. Jin and X. Chen, Stacking seismic data using local correlation, *Geophysics*, vol.74, no.3, pp.V43-V48, 2009.
[18] R. Ragul, G. Sangeetha, K. Mathiyalagan and H. Zhang, Exponential stability results for stochastic semi-linear systems with Lèvy noise, *International Journal of Innovative Computing, Information and Control*, vol.18, no.6, pp.1929-1940, 2022.
[19] T. Chan, S. Esedoglu, F. Park and A. Yip, Total variation image restoration: Overview and recent developments, in *Handbook of Mathematical Models in Computer Vision*, N. Paragios, Y. Chen and O. Faugeras (eds.), Boston, MA, Springer, 2006.
[20] A. Gholami, Nonlinear multichannel impedance inversion by total-variation regularization, *Geophysics*, vol.80, no.5, pp.R217-R224, 2015.
[21] B. Cai, W. Liu and Z. Zheng, An improved nonlocal mean denoising algorithm, *Pattern Recognition and Artificial Intelligence*, vol.29, no.1, pp.1-10, 2016.
[22] Y. Zhao and Q. Huang, Image enhancement of robot welding seam based on wavelet transform and contrast guidance, *International Journal of Innovative Computing, Information and Control*, vol.18, no.1, pp.149-159, 2022.
[23] S. Fomel and Y. Liu, Seislet transform and seislet frame, *Geophysics*, vol.75, no.3, pp.V25-V38, 2010.
[24] Y. Liu, Y. Li, H. Lin and H. Ma, An amplitude-preserved time-frequency peak filtering based on empirical mode decomposition for seismic random noise reduction, *IEEE Geoscience and Remote Sensing Letters*, vol.11, no.5, pp.896-900, 2014.
[25] J. L. Gómez and D. R. Velis, A simple method inspired by empirical mode decomposition for denoising seismic data, *Geophysics*, vol.81, no.6, pp.V403-V413, 2016.
[26] H. Andrews and C. Patterson, Singular value decompositions and digital image processing, *IEEE Transactions on Acoustics, Speech, and Signal Processing*, vol.24, no.1, pp.26-53, 1976.
[27] X. Wang, J. Chen, L. Gao and W. Chen, An iterative zero-offset VSP wavefield separating method based on the error analysis of SVD filtering, *IEEE Geoscience and Remote Sensing Letters*, vol.15, no.8, pp.1164-1168, 2018.
[28] J. Mendel, White-noise estimators for seismic data processing in oil exploration, *IEEE Transactions on Automatic Control*, vol.22, no.5, pp.694-706, 1977.
[29] W. Zhu, S. M. Mousavi and G. C. Beroza, Seismic signal denoising and decomposition using deep neural networks, *IEEE Transactions on Geoscience and Remote Sensing*, vol.57, no.11, pp.9476-9488, 2019.
[30] N. Djarfour, J. Ferahtia, F. Babaia, K. Baddari and M. Farfour, Seismic noise filtering based on generalized regression neural networks, *Computer & Geosciences*, vol.69, pp.1-9, 2014.
[31] K. T. Spikes, N. Tisato, T. E. Hess and J. W. Holt, Comparison of geophone and surface-deployed distributed acoustic sensing seismic data, *Geophysics*, vol.84, no.2, pp.A25-A29, 2019.
[32] M. Intraraprasit and O. Chitsobhuk, Filter pruning based on local gradient activation mapping in convolutional neural networks, *International Journal of Innovative Computing, Information and Control*, vol.19, no.6, pp.1697-1715, 2023.
[33] X. Dong, T. Zhong and Y. Li, New suppression technology for low-frequency noise in desert region: The improved robust principal component analysis based on prediction of neural network, *IEEE Transactions on Geoscience and Remote Sensing*, vol.58, no.7, pp.4680-4690, 2020.

[34] T. Wang, Z. Hu and H. Zhou, Unsupervised feature selection with Hilbert-Schmidt independence criterion Lasso, *International Journal of Innovative Computing, Information and Control*, vol.19, no.3, pp.927-939, 2023.

[35] K. Zhang, W. Zuo, Y. Chen, D. Meng and L. Zhang, Beyond a Gaussian denoiser: Residual learning of deep CNN for image denoising, *IEEE Transactions on Image Processing*, vol.26, no.7, pp.3142-3155, 2017.

[36] T. Zhong, M. Cheng, X. T. Dong, Y. Li and N. Wu, Seismic random noise suppression by using deep residual U-Net, *Journal of Petrolum Science and Engineering*, vol.209, 109901, 2022.

[37] Y. Zhao, Y. Li, X. Dong and B. Yang, Low-frequency noise suppression method based on improved DnCNN in desert seismic data, *IEEE Geoscience and Remote Sensing Letters*, vol.16, no.5, pp.811-815, 2019.

[38] H. Ma, H. Yao, Y. Li and H. Wang, Deep residual encoder-decoder networks for desert seismic noise suppression, *IEEE Geoscience and Remote Sensing Letters*, vol.17, no.3, pp.529-533, 2020.

[39] O. M. Saad and Y. Chen, A fully unsupervised and highly generalized deep learning approach for random noise suppression, *Geophysical Prospecting*, vol.69, no.4, pp.709-726, 2021.

[40] I. Goodfellow, Generative adversarial nets, *Proc. of the 27th International Conference on Neural Information Processing Systems (NIPS'14)*, pp.2672-2680, 2014.

[41] Y. Li, H. Wang and X. Dong, The denoising of desert seismic data based on cycle-GAN with unpaired data training, *IEEE Geoscience and Remote Sensing Letters*, vol.18, no.11, pp.2016-2020, 2021.

[42] Y. Zhao, Y. Li and B. Yang, Low-frequency desert noise intelligent suppression in seismic data based on multiscale geometric analysis convolutional neural network, *IEEE Transactions on Geoscience and Remote Sensing*, vol.58, no.1, pp.650-665, 2020.

[43] X. Gao, L. Tu, J. Li and X. Li, Automatic classification algorithm of astronomical objects based on improved ResNet, *International Journal of Innovative Computing, Information and Control*, vol.19, no.2, pp.579-596, 2023.

[44] G. Huang, Z. Liu, L. Van Der Maaten and K. Q. Weinberger, Densely connected convolutional networks, *Proc. of the IEEE Conference on Computer Vision and Pattern Recognition (CVPR)*, pp.4700-4708, 2017.

[45] K. He, X. Zhang, S. Ren and J. Sun, Identity mappings in deep residual networks, *European Conference on Computer Vision*, pp.630-645, 2016.

[46] S. Jégou, M. Drozdzal, D. Vazquez, A. Romero and Y. Bengio, The one hundred layers Tiramisu: Fully convolutional DenseNets for semantic segmentation, *Proc. of the IEEE Conference on Computer Vision and Pattern Recognition (CVPR)*, pp.11-19, 2017.

[47] S. M. Mousavi, W. L. Ellsworth, W. Zhu and G. C. Beroza, Earthquake transformer – An attentive deep-learning model for simultaneous earthquake detection and phase picking, *Nature Communications*, vol.11, no.1, 3952, 2020.

[48] C. Tian, Y. Xu, Z. Li, W. Zuo and H. Liu, Attention-guided CNN for image denoising, *Neural Networks*, vol.124, pp.117-129, 2020.

[49] T. Zhong, M. Cheng, X. Dong and N. Wu, Seismic random noise attenuation by applying multiscale denoising convolutional neural network, *IEEE Transactions on Geoscience and Remote Sensing*, vol.60, 2022.

Author Biography

Tie Zhong received the B.S., M.S., and Ph.D. degrees in Communication Engineering from Jilin University, Jilin, Jilin, China, in 2006, 2008 and 2016, respectively. He is currently an Associate Professor in the Department of Communication Engineering, School of Electrical Engineering, Northeast Electric Power University, Jilin, Jilin, China. His research interests include modern signal processing techniques, weak signal process theory, and intelligent information processing.

Hang Yu received his bachelor's degree in Communication Engineering from Northeast Electric Power University, Jilin, China, in 2021. He is studying for a master's degree in Northeast Electric Power University, Jilin, China. His main research interest covers modern signal processing.

Wei Wang received the B.S. and M.S. degrees in Geological Resources and Geological Engineering from China University of Petroleum (Beijing), Beijing, China, in 2015 and 2018, respectively. He is currently working in the Institute of Geophysics, Northwest Branch of China Petroleum Exploration and Development Research Institute. His research interests include intelligent geophysical exploration, signal processing, and software development.

Shiqi Dong received the B.Sc. degree in Applied Geophysics and the Ph.D. degree in Geo-exploration and Information Technology from Jilin University, China, in 2016 and 2021, respectively. He is currently an Associate Professor in the School of Electrical Engineering, Northeast Electric Power University, Jilin, China. He has been a visiting student in Massachusetts Institute of Technology from August-October in 2019. His current research interests include full waveform inversion, tunnel advanced prediction and deep learning.